Chapter 2

Investigation of structure-reactivity relationships of iron-based water oxidation catalysts with macrocyclic tetraaza-type ligands – an online electrochemical mass spectrometry approach

*The use of on-line electrochemical mass spectrometry in combination with classical electroanalytical techniques makes it possible to distinguish between competing reactions such as water oxidation and the formation of carbon dioxide at high electrochemical potentials. In this chapter, a selection of three different iron complexes based on the macrocyclic tetraaza-type ligand cyclam is examined using this methodology. For the complex cis-[Fe(cyclam)Cl_2]Cl (**1**) water oxidation activity was found which is in agreement with previous studies that predict iron complexes based on neutral amine ligands with two vacant coordination sites in cis configuration to be active catalysts for water oxidation. The complex [Fe(cyclamacetate)Cl] (**2**) bearing an additional 5^{th} donor ligand in axial position in the form of an acetate group was also found to be an active catalyst for the water oxidation reaction. Meanwhile, the complex trans-[Fe(cyclam)Cl_2] (**3**) which was predicted to be inactive for water oxidation indeed shows very little catalytic activity up until 2.0 V under the same conditions. The results presented in this chapter suggest the presence of a strong correlation between the electronic structure of the iron centre and the observed water oxidation activity.*

Results presented in this chapter have been published previously as a communication style paper: K.G. Kottrup and D.G.H. Hetterscheid, *Chem. Commun.* **2016,** *52*, 2643-2646.

2.1 Introduction

Since fossil fuel reserves are dwindling and CO_2 emissions from fossil fuel consumption contribute to human-made climate change, new technologies are needed to ensure a sustainable energy future. To produce chemical fuels in a sustainable way, electrons are needed in order to reduce substrates such as CO_2 or protons to fuel. A cheap and abundant source of electrons is water, however, this requires a catalyst for the water oxidation reaction. In order to ultimately achieve fuel production on a global scale by means of oxidizing water, a water oxidation catalyst needs to be not only sufficiently efficient and robust but also made from affordable and abundant materials. While excellent catalysts have been developed based on iridium and ruthenium,[1-4] these materials are too scarce and too expensive to be implemented on a large scale. To address this issue, in recent years more and more attention has been given to the development of new catalysts based on more abundant first-row transition metals such as iron, cobalt, nickel, manganese and copper.[5-6] Of those elements, iron in particular has received a lot of interest due to its ability to access a wide range of oxidation states and its importance in oxygen-binding systems in nature.

However, the structure-reactivity relationships that enable efficient, low over-potential water oxidation catalysis based on iron, which are important for the design of new and efficient catalysts, are still not fully understood. In 2011, Fillol et al. reported on a series of iron-based water oxidation catalysts with tetradentate amine ligands.[7] Their key finding was that those complexes which have two vacant coordination sites in *cis*-configuration are active water oxidation catalysts while a structure with two vacant coordination sites in *trans*-positions leads to a catalytically inactive complex. In contrast to that, Collins et al. reported in 2010 that iron-TAML complexes which do not have two vacant sites in *cis*-positions do show water oxidation activity – albeit short lived – with remarkably high turnover frequencies.[8] This juxtaposition already indicates that other factors must also play a role in determining the catalytic activity of a given complex aside from its geometry. Fillol and co-workers were able to support their proposed mechanism involving *cis* vacant sites through subsequent DFT calculations.[9] However, in a follow-up publication they reported that the use of the sacrificial oxidant cerium(IV) ammonium nitrate (CAN) to drive the reaction results in the formation of a Fe–μ-O–Ce species,[10] suggesting a direct involvement of the oxidant in the catalytic mechanism.

Intrigued by these findings we synthesized a selection of iron-based complexes with different structural motifs and investigated their redox behaviour and their water oxidation capabilities by means of electroanalytical techniques.

Despite their possibly limited stability under highly oxidative conditions, macrocyclic cyclam-based ligands (Fig. 2.1) were selected in this study for complexation to iron because such complexes are expected to be relatively stable towards ligand dissociation and the corresponding iron complexes bearing vacant sites in *cis*- and *trans*-configuration have been synthesized[11] and used in oxidation chemistry[12] previously. Furthermore, previous studies have suggested that macrocyclic ligands can enable catalytic water oxidation activity of iron complexes in some cases.[13] The results of the experiments discussed in this chapter show no considerable catalytic activity for *trans*-[Fe(cyclam)Cl_2] (**3**). In contrast, the complexes *cis*-[Fe(cyclam)Cl_2]Cl (**1**) and [Fe(cyclamacetate)Cl] (**2**) are found to be capable of catalyzing the water oxidation reaction. To the best of our knowledge, [Fe(cyclamacetate)Cl] (**2**) is the first iron-based water oxidation electrocatalyst with only one free coordination site which is active in aqueous media.

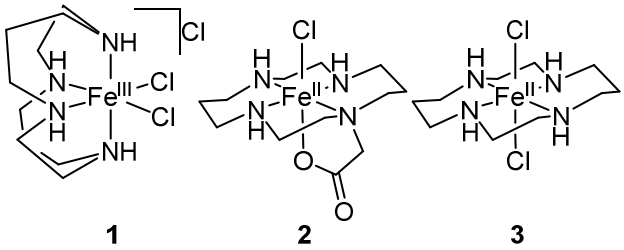

1 **2** **3**

Figure 2.1: Structures of complexes **1**, **2** and **3**

2.2 Results and Discussion

2.2.1 Synthesis and characterization

Cis-[Fe(cyclam)Cl_2]Cl (**1**) was synthesized according to literature procedures.[11] The complex was isolated as orange crystals of high purity, which was confirmed by elemental analysis. Whereas complex **1** was obtained as a Fe^{III} species, the complexes **2** and **3** were isolated as Fe^{II} species and oxidized to the Fe^{III} species *in situ* prior to electrochemical experiments.

Complex **2** can be isolated as a white powder and oxygen-free solutions of **2** in acetonitrile, water and methanol are all colourless which is indicative of a high-

spin Fe^{II} configuration. Upon exposure to air, solutions of complex **2** quickly turn (dark) yellow indicating oxidation from Fe^{II} to Fe^{III}. EPR-measurements indicate that complex **2** is EPR-silent (X-band), which is not uncommon for high-spin iron(II) species.[14] After exposure of the aqueous solution to air, the oxidized complex yields an EPR spectrum with three distinct g-values of 2.48, 2.21 and 1.89 (Fig. A.1a, Appendix A) which is in good agreement with previous reports.[15] For the C=O stretch vibration of the carboxyl group, a shift of 139 cm^{-1} was observed by comparing the IR spectra of the ligand and complex **2**, suggesting that the acetate group coordinates to the iron-centre in the solid state (Fig. A.2, Appendix A).

The Fe^{III} *trans*-analogue of complex **1** has been reported previously.[11] However, the complex was isolated as a $[FeCl_4]^-$ salt and attempts to recrystallize it with other counter-ions proved to be difficult. To avoid the presence of any $[FeCl_4]^-$ in the catalytic experiments, a different approach was taken instead. *Trans*-$[Fe(cyclam)Cl_2]$ (**3**) was synthesized as the Fe^{II} species in a procedure analogous to that of complex **2** and was isolated as a light pink powder.

Previous reports show that the iron-centre in complex **1** is in the high-spin state whereas the analogous *trans*-species has a low-spin Fe^{III} centre due to a Jahn-Teller distortion.[11] In the EPR spectrum obtained for the oxidized form of complex **3** (Fig. A.1b, Appendix A), the predominant signal shows g-values of 2.39, 2.24 and 1.93, which suggests that the major species present in solution has a similar structure to the oxidized form of complex **2**, indicating the desired *trans*-configuration. Next to the main signal, the EPR spectrum of **3** also shows 2 additional minor signals which might arise from traces of the *cis*-conformer or traces of residual $FeCl_2$ in the sample. The presence of chloride ions and glycerol in the sample further complicate the system and may cause unexpected signals.

UV-vis experiments of complexes **1** and **3** in aqueous solution show that the absorption spectrum of complex **1** remains stable over the course of at least 90 minutes while the spectrum of complex **3** changes notably, most likely due to oxidation from the Fe^{II} to the Fe^{III} oxidation state in air. Comparison of the UV-vis spectra of both complexes also shows that the spectra remain distinctly different for both complexes, showing that no significant interconversion between the *cis* and the *trans* species takes place under these conditions (Fig. A.3, Appendix A).

2.2.2 Electrochemical studies

2.2.2a General

The redox behaviour and catalytic activity of *cis*-[Fe(cyclam)Cl_2]Cl (**1**), [Fe(cyclamacetate)Cl] (**2**) and *trans*-[Fe(cyclam)Cl_2] (**3**) were studied via electroanalytical techniques using a pyrolytic graphite (PG) working electrode in aqueous solutions of either unbuffered 0.1 M $NaClO_4$ or 0.1 M phosphate buffer (pH 7.5). Electrochemical experiments using acidic media (pH 1) yielded poor results and preliminary tests with chemical oxidants showed only low single digit turnover numbers and rapid catalyst deactivation. We refrained from catalytic studies under very alkaline conditions to avoid formation of iron oxide which could potentially obscure catalytic activity of the molecular complexes.[16] To investigate whether the catalytic results depend on the electrode of choice, we tested working electrodes made from gold as well as PG. Gold electrodes form a layer of gold oxide on the surface, starting around 1.2–1.3 V vs. a reversible hydrogen electrode (RHE). The gold oxide surface is not stable in the presence of chloride ions, resulting in the formation of $[AuCl_4]^-$ which gives rise to a large current between 1.2 and 1.6 V vs. RHE which potentially obscures other features in the CV (Fig. 2.2). Additionally, it has been proposed that the presence of halide ions can interfere with the mechanism of the water oxidation reaction.[17] Since isolation of complexes **1**–**3** with different counter ions proved to be difficult, PG was selected as the best electrode material for our purposes since the presence of chloride ions seems to have no significant effect on the resulting CV (Fig. 2.3).

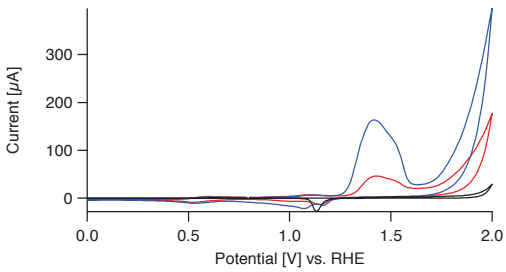

Figure 2.2: Voltammogram showing a blank gold working electrode (black) and a gold working electrode in the presence of complex **1** without (red) and with the addition of 6 eq. NaCl (blue). The current of the oxidation peak at ~1.4 V vs. RHE correlates directly with the concentration of Cl^- ions. Conditions: 0.1 M $NaClO_4$, 1.1 mM complex **1**, scan rate 10 mV/s.

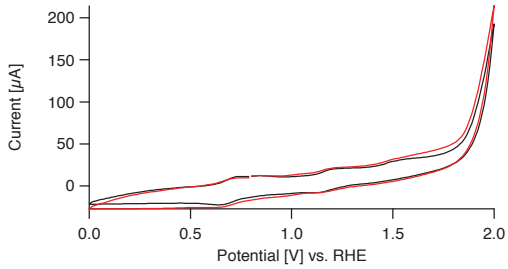

Figure 2.3: Voltammograms of complex **1**, using a PG working electrode with and without added NaCl. The black line represents the voltammogram of complex **1** using a PG working electrode, the red line represents the voltammogram after the addition of 6 eq. NaCl. In contrast to the observed chloride oxidation on gold (cf. Fig. 2.2), the addition of several equivalents of NaCl produces no significant difference in the voltammogram recorded for complex **1** with a PG working electrode. Conditions: 0.1 M $NaClO_4$, 1.1 mM complex **1**, scan rate 10 mV/s.

2.2.2b Electrochemical studies in unbuffered solution

In an unbuffered 0.1 M $NaClO_4$ solution, complex **1** shows a reversible wave at 0.7 V which is assigned to the $Fe^{II/III}$ couple (Fig. 2.4a). At 1.2 V vs. RHE another redox couple can be seen in the CV as well as an irreversible oxidative wave at 1.5 V vs. RHE. Starting at about 1.8 V, a sharp increase in current is observed in the voltammogram (Fig. 2.4b).

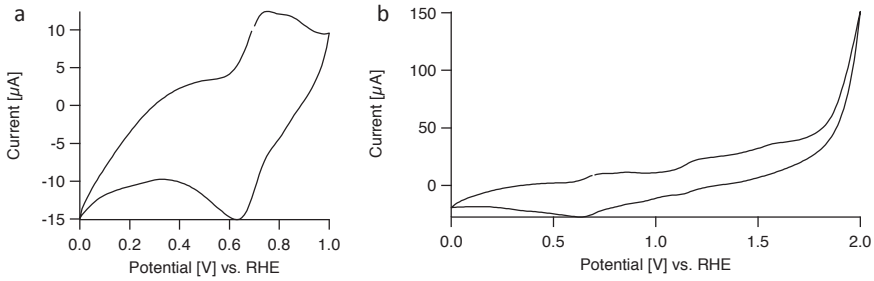

Figure 2.4: Results of a CV measurement of 1.1 mM complex **1** using a PG working electrode in a 0.1 M $NaClO_4$ solution measured at 10 mV/s with a starting potential of 0.7 V vs. RHE with a scan range of (a) 0.0 to 1.0 V vs. RHE and (b) 0.0 to 2.0 V vs. RHE.

To identify the products formed upon electrochemical oxidation and to determine the onset potentials of these reactions, online electrochemical mass spectrometry (OLEMS) was used. In OLEMS measurements, the *m/z* traces for selected gaseous products, sampled close to the electrode surface in solution, are recorded during electrochemical measurements. In chronoamperometry measurements at 1.9 V, immediate O_2 evolution was detected via OLEMS, without any induction period or any CO_2 formation preceding the onset of O_2 evolution (Fig. 2.5a). This indicates that the catalytic reaction is mediated by a molecular species. The mass trace of

O_2 was also measured as a function of potential to determine the onset potential for O_2 evolution. Following the recorded traces for *m/z* = 32 (Fig. 2.6a), an increase in signal can be observed indicating the formation of dioxygen starting near 1.8 V which correlates with the sharp onset of oxidative current seen in the CV. Additionally, the trace of *m/z* = 44 was measured to monitor the formation of CO_2 which is expected to be a product of oxidative decomposition of the ligand. Comparison of the mass traces shows that the formation of CO_2 starts at lower potentials than the evolution of O_2 (Fig. 2.6a).

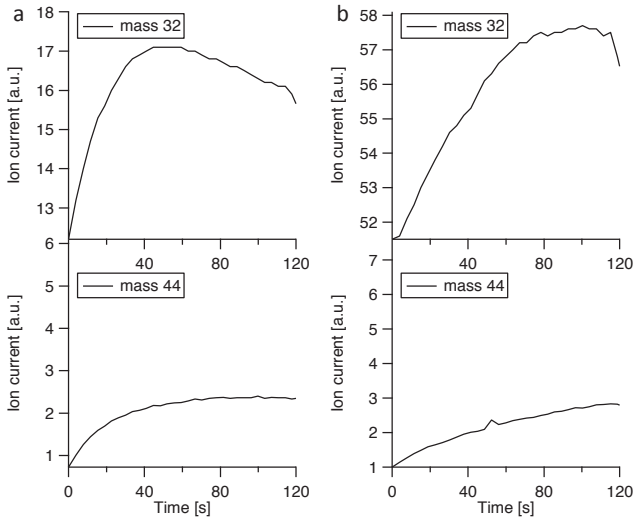

Figure 2.5: *m/z* traces of O_2 (top) and CO_2 (bottom) recorded during chronoamperometry measurements in a 0.1 M $NaClO_4$ solution with 1.1 mM of (a) complex **1** at 1.9 V vs. RHE and (b) complex **2** at 2.0 V vs. RHE.

The formation of CO_2 points to a weakness of the ligand framework under these oxidizing conditions. This finding is in line with the results of previous reports of iron-based molecular catalysts for water oxidation which generally show low Faradaic efficiencies or low turn-over numbers.[7, 13, 18] It has to be noted that the observed CO_2 may originate at least in part from oxidation of the carbon electrode itself, mediated by the presence of high-valent iron oxo-species. To get further insight into the catalyst stability, cyclic voltammetry was performed in the presence of complex **1**, followed by chronoamperometry for 180 s at 1.9 V vs. RHE, immediately followed by another cyclic voltammetry run, starting with a cathodic scan from 2.0 V to 0.0 V vs. RHE. The voltammogram recorded before and after chronoamperometry experiment are almost superimposable, except for an increase in reductive current between 0.5 V and 0.0 V vs. RHE (Fig. 2.7), which

most likely stems from the reduction of the dioxygen produced during the chronoamperometry experiment and a slightly increased oxidative current beyond 1.5 V which is ascribed to oxidative modification of the PG electrode under high potential conditions. Aside from the reductive current below 0.5 V and a slightly higher oxidative current beyond 1.5 V, the basic features of the CV are identical before and after the chronoamperometry experiment, indicating that the complex remains mostly intact. It is to be expected that diffusion of unreacted complex from the bulk solution to the electrode surface will mask the effect of catalyst decomposition to some extent. However, from these results the catalyst appears to be reasonably stable within the time span of the experiments.

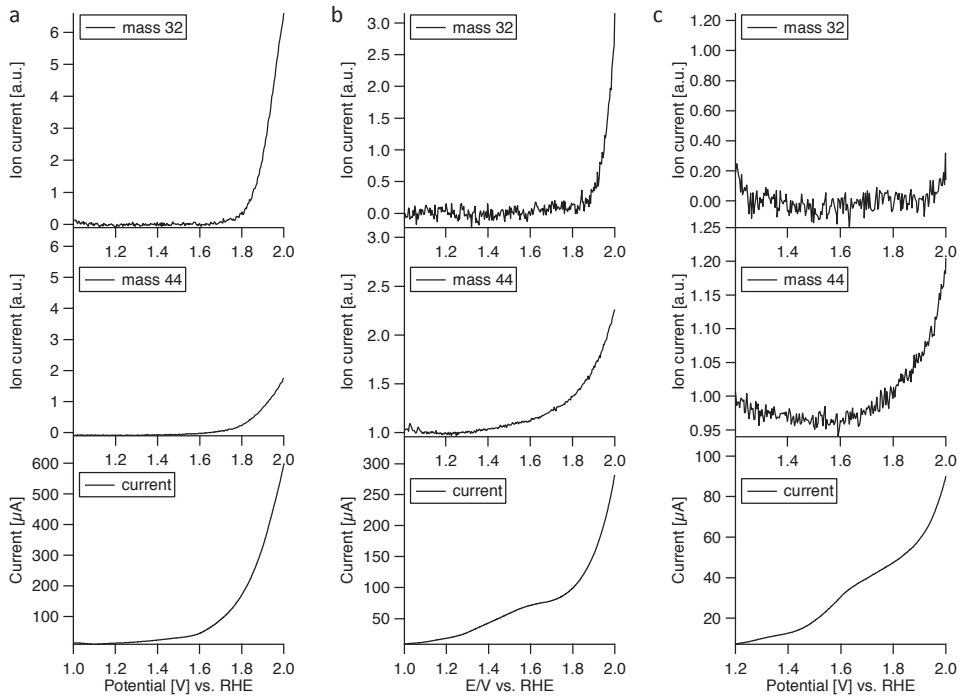

Figure 2.6: Shown are the *m/z* traces of O_2 (top), CO_2 (middle) and the corresponding current (bottom) of OLEMS measurements recorded during electrochemical potential cycling at 1 mV/s. For the sake of clarity, only the forward scan of each experiment is depicted. Conditions: (a) 1.1 mM complex **1** in a 0.1 M $NaClO_4$ solution, scanning between 1.0 and 2.0 V vs. RHE, starting at 1.0 V vs. RHE. (b) 1.1 mM complex **2** in a 0.1 M $NaClO_4$ solution, scanning between 1.0 and 2.0 V vs. RHE, starting at 1.0 V vs. RHE. (c) 1.1 mM complex **3** in a 0.1 M $NaClO_4$ solution, scanning between 1.2 and 2.0 V vs. RHE, starting at 1.2 V vs. RHE.

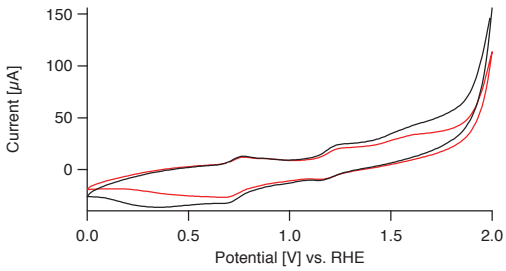

Figure 2.7: Comparison of voltammograms of 1.1 mM complex **1** in a 0.1 M $NaClO_4$ solution at a scan rate of 10 mV/s before (red) and after (black) chronoamperometry (180 s at 1.9 V).

Similar to complex **1**, complex **2** shows a reversible $Fe^{II/III}$ redox-couple at 0.7 V (Fig. 2.8a). Starting at 1.3 V, an irreversible oxidative current can be observed in the voltammogram with a sharp increase in current starting at 1.8 V (Fig. 2.8b).

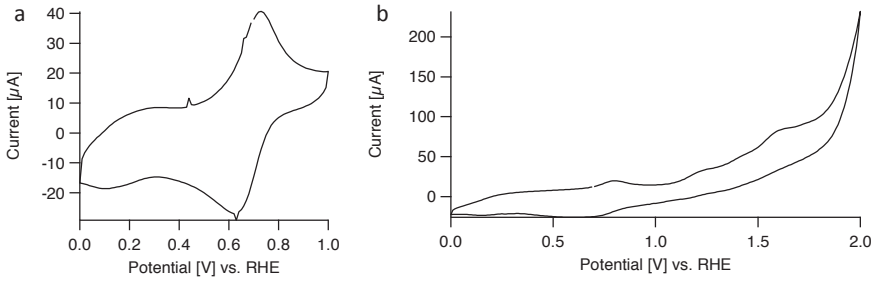

Figure 2.8: Results of a CV measurement of 1.1 mM complex **2** using a PG working electrode in a 0.1 M $NaClO_4$ solution measured at 10 mV/s with a starting potential of 0.7 V vs. RHE with a scan range of (a) 0.0 to 1.0 V vs. RHE and (b) 0.0 to 2.0 V vs. RHE.

Chronoamperometry measurements for complex **2** at 2.0 V again show immediate O_2 evolution without any sign of an induction period or CO_2 formation preceding the evolution of O_2 (Fig. 2.5b). Measuring the mass trace of O_2 as a function of potential shows that the onset of O_2 evolution correlates with the sharp increase in oxidative current at 1.8 V (Fig. 2.6b). The current observed between 1.3 and 1.8 V correlates with CO_2 formation (Fig. 2.6b).

The reversible $Fe^{II/III}$ couple of complex **3** was observed at 0.9 V in a 0.1 M $NaClO_4$ solution (Fig. 2.9a). From 1.5 V onwards, an irreversible oxidative current can be observed with a sharp increase at 1.9 V (Fig. 2.9b). In the OLEMS measurements of complex **3**, detectable amounts of CO_2 are observed beyond 1.6 V and the irreversible oxidative current starting at 1.9 V can be attributed to O_2 evolution (Fig. 2.6c).

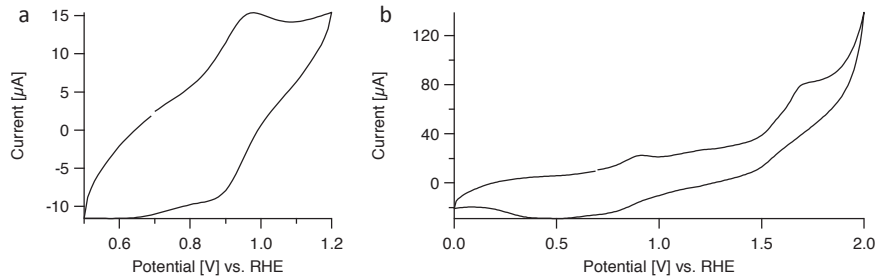

Figure 2.9: Results of a CV measurement of complex 1.1 mM **3** using a PG working electrode in a 0.1 M $NaClO_4$ solution measured at 10 mV/s with a starting potential of 0.7 V vs. RHE with a scan range of (a) 0.0 to 1.0 V vs. RHE and (b) 0.0 to 2.0 V vs. RHE.

By comparing the relative amounts of O_2 and CO_2 that are observed in the OLEMS measurements, it appears that the catalytic activity of complex **3** is substantially lower than that of **1** and **2**. Considering the presence of some high-spin Fe^{III} species in aqueous solutions of **3** (Fig. A.1b, Appendix A), one might wonder whether the *trans*-complex is active at all or whether the observed catalytic activity for **3** is merely an artefact, due to small amounts of *cis*-complex present in solution.

2.2.2c Electrochemical studies in pH 7.5 phosphate buffer

For applications of a catalytic system at neutral pH, it is relevant to know whether the catalyst is active in the presence of a pH buffer. Both complexes **1** and **3** are fully deactivated in phosphate-containing media. Both complexes show a cathodic shift of the $Fe^{II/III}$ redox couple to 0.3 V vs. RHE (Fig. 2.10a-b), indicating a strong interaction with phosphate.

OLEMS measurements of complex **1** in a 0.1 M phosphate buffer solution show a similar CO_2 formation profile as seen previously in an unbuffered $NaClO_4$ solution but no signs of O_2 evolution up to 2.0 V (Fig. 2.11a). At low scan rates (1 mV/s) in the presence of phosphate, complex **3** forms a deposit of an unidentified blue material on the surface of the PG electrode (Fig. A.4, Appendix A). The blue deposit itself is active for water oxidation (Fig. 2.11b), albeit with an onset for O_2 evolution at around 1.9 V. In the OLEMS experiment of complex **3** in phosphate buffer, a steady increase in the dioxygen signal between each consecutive scan can be seen (Fig. 2.12) as a result of the slow formation of the deposit during high-potential conditions in each scan.

In the presence of 0.1 M phosphate (pH 7.5), complex **2** shows redox couples at 0.3 V and 0.6 V, indicating only partial inhibition by phosphate. (Fig. 2.10c). An

onset for O_2 evolution was observed at 1.9 V in an OLEMS measurement (Fig. 2.11c).

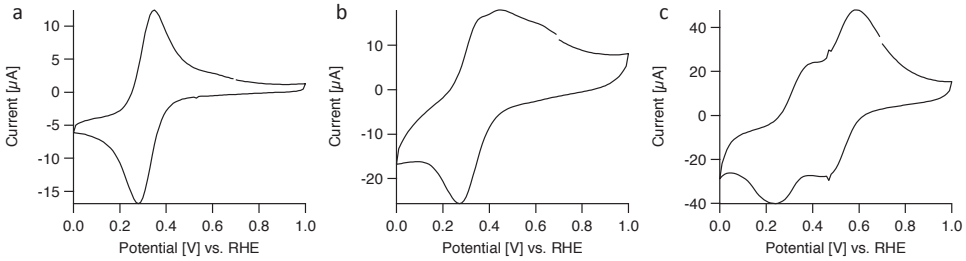

Figure 2.10: Results of CV experiments, showing the $Fe^{II/III}$ redox couples of complex **1** (a), complex **3** (b) and complex **2** (c), each in a 0.1 M phosphate buffer solution (pH 7.5). All three CVs were recorded at 10 mV/s between 0.0 and 1.0 V vs. RHE with a starting potential of 0.7 V vs. RHE.

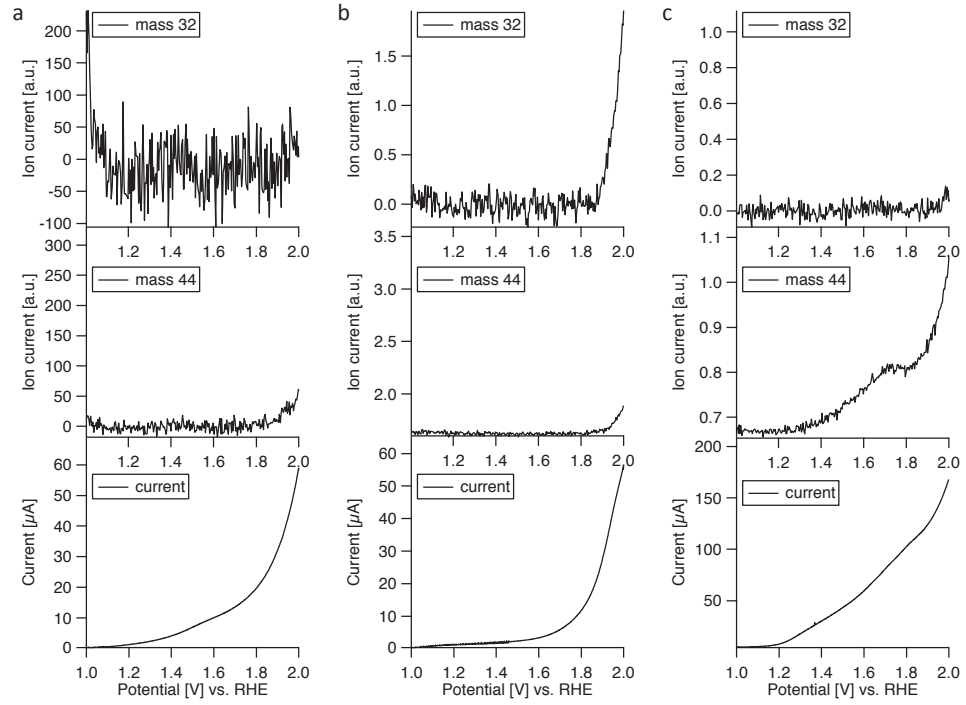

Figure 2.11: Results of several OLEMS experiments recorded during electrochemical potential cycling between 1.0 and 2.0 V vs. RHE at 1 mV/s, starting at 1.0 V vs. RHE. Shown are the *m/z* traces of O_2 (top) and CO_2 (middle) and the corresponding current (bottom) recorded. For the sake of clarity, only the forward scan of each experiment is depicted. The graphs correspond to: (a) 1.1 mM complex **1** in a 0.1 M phosphate buffer solution (pH 7.5), (b) the blue deposit which was formed while cycling the potential 3 times beween 1.0 and 2.0 V vs. RHE at 1 mV/s, starting at 1.0 V vs. RHE in the presence of 1.1 mM complex **3** in 0.1 M phosphate buffer solution (pH 7.5) and (c) 1.1 mM complex **3** in a 0.1 M phosphate buffer solution (pH 7.5)

In contrast to complex **3**, complexes **1** and **2** showed no visible signs of deposition of (blue) material onto the electrode surface even after prolonged potential cycling between 1.0 and 2.0 V at a scan rate of 1 mV/s. Electrodes which were taken out of a phosphate buffer solution containing complex **1** or **2**, rinsed with Milli-Q water and placed in a fresh phosphate buffer solution of identical concentration and pH did not produce any significant current above the PG background.

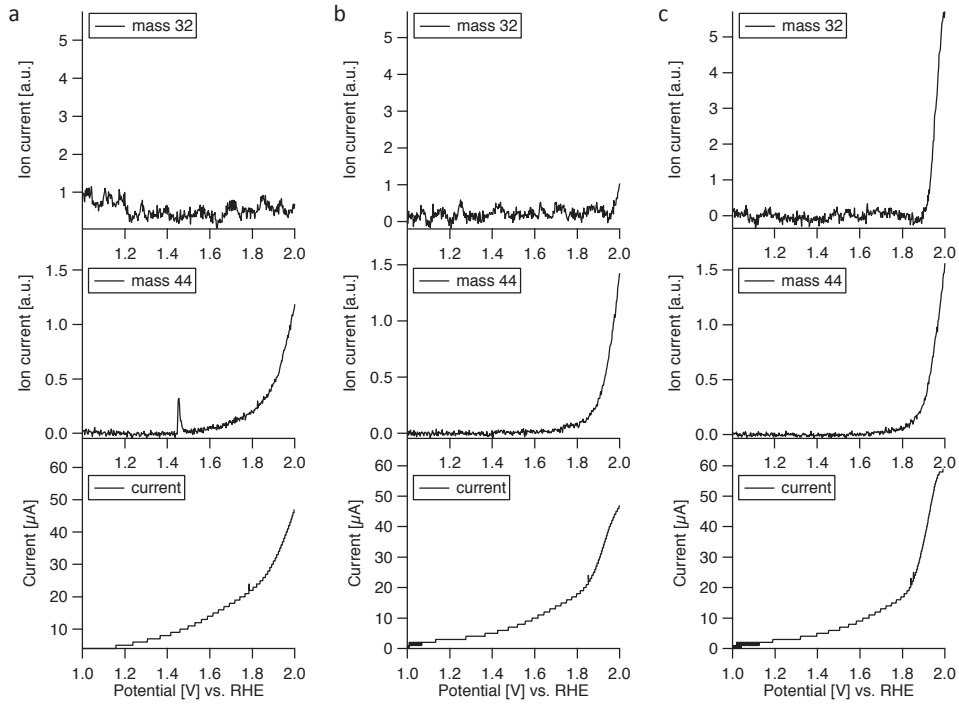

Figure 2.12: Three scans of an OLEMS experiment of 1.5 mM complex **3** in a 0.1 M phosphate buffer solution (pH 7.5). Shown are the *m/z* traces of O_2 (top), CO_2 (middle) and the corresponding current (bottom). For the sake of clarity, only the forward scan of each experiment is depicted. (a) Scan 1 of 3 between 1.0 and 2.0 V vs. RHE, recorded at 1 mV/s, starting at 1.0 V vs. RHE. (b) Scan 3 of 3 between 1.0 and 2.0 V vs. RHE, recorded at 1 mV/s, starting at 1.0 V vs. RHE. (c) Scan 3 of 3 between 1.0 and 2.0 V vs. RHE, recorded at 1 mV/s, starting at 1.0 V vs. RHE.

2.3 Conclusions

The use of on-line mass spectrometry techniques makes it possible to differentiate between catalytic current and current caused by side-reactions such as CO_2 formation. This offers valuable new insights for studying water oxidation

catalysts and can help to alleviate some of the ambiguity caused by the use of sacrificial chemical oxidants.

While *cis*-[Fe(cyclam)Cl_2]Cl (**1**) displays water oxidation activity which was expected based on the results previously reported for comparable molecular iron-based catalysts, [Fe(cyclamacetate)Cl] (**2**) is the first water oxidation catalyst of its kind to operate in aqueous media. In contrast to complexes **1** and **3**, complex **2** was found to be more tolerant towards the presence of phosphate buffer.

In the three complexes investigated in this study, water oxidation activity was demonstrated to be enabled both by the motif of *cis* vacant sites as well as a fifth donor ligand in axial position. Both structural motifs seem to affect the electronic structure of the corresponding complexes in a similar way, leading to a cathodic shift of the $Fe^{II/III}$ redox event compared to *trans*-[Fe(cyclam)Cl_2] (**3**) and enabling water oxidation at lower onset potentials. These results highlight the importance of the electronic features as a design principle for creating new iron-based electrocatalysts for the water oxidation reaction.

The observation of CO_2 formation during the measurements could be indicative of oxidative decomposition of the ligand structure under catalytic conditions, suggesting the need for a more oxidatively stable ligand framework. However, the presence of a carbon-based electrode material makes it difficult to determine the source of the CO_2.

2.4 Experimental

2.4.1 General

All chemicals were used as received and without further purification. Cyclam was obtained from Alfa Aesar and iodoacetic acid was obtained from Acros Organics. $FeCl_2 \cdot 4H_2O$ was obtained from Sigma Aldrich and stored under argon. Cylcamacetate·4HCl and *cis*-[Fe(cyclam)Cl_2]Cl (**1**) were synthesized according to literature procedures.[11, 19] The syntheses of complexes **2** and **3** were performed using standard Schlenk-line techniques. Acetonitrile was degassed using standard freeze-pump-thaw protocols.

IR spectra were recorded on a Perkin Elmer UATR (Single Reflection Diamond) Spectrum Two device. Mass spectra were measured on a Finnigan Aqua Mass ESI spectrometer. NMR spectra were measured on a Bruker DPX 300 spectrometer. EPR spectra were recorded on a Bruker EMXplus X-band spectrometer. Elemental analyses were performed by Mikroanalytisches Laboratorium Kolbe in Germany.

2.4.2 Electrochemical experiments

Electrochemical measurements were performed in a custom made single-compartment glass cell on Ivium potentiostats, operated by IviumSoft software, using a three-electrode setup. The working electrode was a pyrolytic graphite (PG) disc with a (geometric) surface area of 0.2 cm^2 used in hanging meniscus configuration. A large surface area gold plate was used as a counter electrode. The reference electrode was a reversible hydrogen electrode (RHE) made up of a platinum mesh in H_2-saturated electrolyte at the same pH as the working solution. The cell and the reference electrode were connected via a Luggin capillary. A fresh PG surface was prepared before each experiment by polishing the working electrode with sandpaper and subsequent removal of excess debris by sonication in Milli-Q water for at least 5 minutes.

All glassware used in electrochemical measurements was routinely cleaned of any organic contamination by boiling in 3:1 mixture of concentrated sulfuric and nitric acid. Prior to each experiment the glassware was cleaned by threefold rinsing and boiling in Milli-Q water. The electrolyte solutions were prepared from p.a. grade chemicals obtained from Merck (Suprapur®) and Milli-Q water.

Prior to measurements, the electrolyte solution was purged of air by bubbling with argon (Linde, Ar 6.0) for at least 20 minutes. During the measurements, the cell was constantly kept under argon flow to prevent air from entering.

Except for preliminary tests with a gold working electrode (Fig. 2.2), all experiments were performed on a PG disc working electrode.

For the OLEMS measurements, the gasses formed at the working electrode were collected via a hydrophobic tip (KEL-F with a porous Teflon plug) in close proximity to the surface of the working electrode and analyzed in a QMS 200 mass spectrometer. A detailed description of the OLEMS setup is available elsewhere.[20] All electrochemical potential cycling in combination with OLEMS was done at a scan rate of 1 mV/s. For the mass spectrometry data recorded via OLEMS during cylic voltammetry measurements, background correction was done by assuming an exponential decay fit (concerns Figures 2.6, 2.11 and 2.12).

2.4.3 Synthesis of [Fe(cyclamacetate)Cl] (**2**)

Cyclamacetate·4HCl (112 mg, 0.28 mmol) was suspended in 5 mL acetonitrile and dissolved upon addition of triethylamine (0.2 mL, 1.42 mmol). Subsequently $FeCl_2 \cdot 4H_2O$ (60 mg, 0.30 mmol) dissolved in 5 mL acetonitrile was added. The mixture was left to stir over night. The white precipitate was subsequently filtered

off, washed with acetonitrile (3 x 5 mL) and dried in vacuo to give **2** as a white solid. Yield: 67 mg (0.19 mmol, 69%)
ESI-MS (1:1 MeOH:H_2O) calcd. for $C_{12}H_{25}ClFeN_4O_2$ $[M]^+$ 348.1; Found: $[M\text{-}Cl]^+$ 313.1, $[M\text{-}Cl+OH]^+$ 330.1, $[M\text{-}Cl+OMe]^+$ 344.2
IR (neat): 1595 cm^{-1} (s, C=O stretch).
Elemental analysis calcd. (%) for $C_{12}H_{25}ClFeN_4O_2$ (348.65 g/mol): C 41.34, H 7.23, N 16.07 Found: C 41.16, H 7.47, N 15.87.

*2.4.4 Synthesis of trans-[Fe(cyclam)Cl_2] (**3**)*

To a suspension of cyclam (40 mg, 0.20 mmol) in 5 mL acetonitrile, $FeCl_2 \cdot 4H_2O$ (40 mg, 0.20 mmol) dissolved in 5 mL acetonitrile was added. The mixture was left to stir over night. The pale pink precipitate was subsequently filtered off, washed with acetonitrile (3 x 5 mL) and dried in vacuo to give **3** as a pale pink solid. Yield: 42 mg (0.13 mmol, 64%)
ESI-MS (MeOH) calcd. for $C_{10}H_{24}Cl_2FeN_4$ $[M]^+$ 326.1; Found: $[M\text{-}H\text{-}Cl]^+$ 290.1, $[M]^+$ 326.0
Elemental analysis calcd. (%) for $C_{10}H_{24}Cl_2FeN_4$ (327.07 g/mol): C 36.72, H 7.40, N 17.13 Found: C 38.31, H 8.08, N 16.48.

*2.4.5 Elemental analysis of cis-[Fe(cyclam)Cl_2]Cl (**1**)*

Elemental analysis calcd. (%) for $C_{10}H_{24}Cl_3FeN_4$ (362.52 g/mol): C 33.13, H 6.67, N 15.45 Found: C 33.33, H 6.50, N 15.38.

2.4.6 Sample preparation

For electrochemical experiments with the *in situ* oxidized complexes **2** and **3**, the respective Fe^{II}-complex was dissolved in air-saturated electrolyte and measured within minutes. In case of EPR experiments, the solution was kept under air for the entire duration. For EPR measurements, glycerol was added to the aqueous solution prior to freezing at 77 K in order to obtain a good glass. In electrochemistry experiments with samples of oxidized complexes **2** and **3**, the electrolyte solution was purged again by bubbling with argon for several minutes after the oxidized complex was added to the cell.
Complete dissolution of crystalline complex **1** was achieved by sonication for at least 20 minutes. Since the dissolution of **1** in 0.1 M $NaClO_4$ solution appears to be substantially slower compared to 0.1 M phosphate buffer, for the experiments in $NaClO_4$ media the complex was dissolved in Milli-Q water instead and

subsequently added to the electrolyte solution. In these experiments, the concentration of electrolyte in the cell was adjusted to account for the resulting dilution. After addition of complex **1**, the electrolyte was purged again by bubbling with argon for several minutes.
In electrochemical experiments described in this chapter, catalyst concentrations of 1.1 mM were used unless otherwise specified.

2.5 Supporting Info

The following supplementary information can be found in Appendix A: Results of EPR measurements of complexes **2** and **3** in frozen aqueous sample at 77 K (Fig. A.1), a comparison of the IR spectra of the free cyclamacetate·4HCl ligand and complex **2** (Fig. A.2), UV-vis spectra of complexes **1** and **3** in aqueous solution (Fig. A.3) and a picture of the blue deposit formed from complex **3** in pH 7.5 phosphate buffer on the surface of a PG electrode (Fig. A.4).

2.6 References

[1] J. D. Blakemore; R. H. Crabtree; G. W. Brudvig, *Chem. Rev.* **2015**, *115*, 12974-13005.
[2] D. G. H. Hetterscheid; J. N. Reek, *Angew. Chem., Int. Ed.* **2012**, *51*, 9740-9747.
[3] X. Sala; I. Romero; M. Rodriguez; L. Escriche; A. Llobet, *Angew. Chem., Int. Ed.* **2009**, *48*, 2842-2852.
[4] D. J. Wasylenko; R. D. Palmer; C. P. Berlinguette, *Chem. Commun.* **2013**, *49*, 218-227.
[5] M. D. Karkas; B. Akermark, *Dalton Trans.* **2016**, *45*, 14421-14461.
[6] A. Singh; L. Spiccia, *Coord. Chem. Rev.* **2013**, *257*, 2607-2622.
[7] J. L. Fillol; Z. Codola; I. Garcia-Bosch; L. Gomez; J. J. Pla; M. Costas, *Nat. Chem.* **2011**, *3*, 807-813.
[8] W. C. Ellis; N. D. McDaniel; S. Bernhard; T. J. Collins, *J. Am. Chem. Soc.* **2010**, *132*, 10990-10991.
[9] F. Acuna-Pares; Z. Codola; M. Costas; J. M. Luis; J. Lloret-Fillol, *Chem. - Eur. J.* **2014**, *20*, 5696-5707.
[10] Z. Codola; L. Gomez; S. T. Kleespies; L. Que, Jr.; M. Costas; J. Lloret-Fillol, *Nat. Commun.* **2015**, *6*, 5865.
[11] R. Guilard; O. Siri; A. Tabard; G. Broeker; P. Richard; D. J. Nurco; K. M. Smith, *J. Chem. Soc., Dalton Trans.* **1997**, 3459-3463.
[12] M. Costas; M. P. Mehn; M. P. Jensen; L. Que, Jr., *Chem. Rev.* **2004**, *104*, 939-986.
[13] B. Zhang; F. Li; F. Yu; H. Cui; X. Zhou; H. Li; Y. Wang; L. Sun, *Chem. - Asian J.* **2014**, *9*, 1515-1518.

[14] G. Mathies; S. D. Chatziefthimiou; D. Maganas; Y. Sanakis; S. Sottini; P. Kyritsis; E. J. Groenen, *J. Magn. Reson.* **2012**, *224*, 94-100.
[15] W. S. Szulbinski; D. H. Busch, *Inorg. Chim. Acta* **1995**, *234*, 143-148.
[16] G. Chen; L. Chen; S. M. Ng; W. L. Man; T. C. Lau, *Angew. Chem., Int. Ed.* **2013**, *52*, 1789-1791.
[17] Z. Chen; J. J. Concepcion; N. Song; T. J. Meyer, *Chem. Commun.* **2014**, *50*, 8053-8056.
[18] Z.-Q. Wang; Z.-C. Wang; S. Zhan; J.-S. Ye, *Appl. Catal., A* **2015**, *490*, 128-132.
[19] M. Studer; T. A. Kaden, *Helv. Chim. Acta* **1986**, *69*, 2081-2086.
[20] A. H. Wonders; T. H. M. Housmans; V. Rosca; M. T. M. Koper, *J. Appl. Electrochem.* **2006**, *36*, 1215-1221.